

DISCOVER: A Solver for Distributional Counterfactual Explanations

Yikai Gu¹, Lele Cao², Bo Zhao³, Lei Lei⁴, Lei You¹

¹Technical University of Denmark, ²Scholar7, ³Aalto University, ⁴Xi'an Jiaotong University

Counterfactual explanations (CE) explain model decisions by identifying input modifications that lead to different predictions. Most existing methods operate at the instance level. Distributional Counterfactual Explanations (DCE) extend this setting by optimizing an optimal transport objective that balances proximity to a factual input distribution and alignment to a target output distribution, with statistical certification via chance constrained bounds. However, DCE relies on gradient based optimization, while many real-world tabular pipelines are dominated by non-differentiable models. We propose DISCOVER, a model-agnostic solver for distributional counterfactual explanations. DISCOVER preserves the original DCE objective and certification while replacing gradient descent with a sparse propose-and-select search paradigm. It exploits a sample-wise decomposition of the transport objective to compute per-row impact scores and enforce a top- k intervention budget, focusing edits on the most influential samples. To guide candidate generation without predictor gradients, DISCOVER introduces an OT-guided cone sampling primitive driven by input-side transport geometry. Experiments on multiple tabular datasets demonstrate strong joint alignment of input and output distributions, extending distributional counterfactual reasoning to modern black box learning pipelines. A code repository is available at <https://github.com/understanding-ml/DCE>.

Correspondence: leiyo@dtu.dk

Date: February 2026



1 Introduction

1.1 Background and Motivations

Counterfactual explanations (CE) are widely used in explainable artificial intelligence (XAI) to provide actionable insights for automated decision systems [Dwivedi et al. \(2023\)](#); [Verma et al. \(2024\)](#). They describe minimal and feasible changes to the input that would lead a model to produce a desired outcome [Wachter et al. \(2017\)](#). Most CE methods operate at the instance level and are designed to provide recourse for a single instance, often incorporating feasibility constraints and user-specific costs [Ustun et al. \(2019\)](#); [Karimi et al. \(2020\)](#) or returning multiple diverse alternatives [Mothilal et al. \(2020\)](#). However, many real-world applications require population-level interventions rather than isolated edits. For example, policy makers may ask how to shift the risk distribution of a subgroup, or financial institutions may seek systematic recourse strategies that remain consistent with the overall data manifold. Existing global or group-level recourse toolkits partially address this issue by aggregating or organizing per-instance actions [Rawal and Lakkaraju \(2020\)](#); [Ley et al. \(2023\)](#), but their objectives remain defined over individual edits

rather than distributions, and they do not directly optimize the shape of the model’s output distribution that stakeholders aim to control. These settings call for distributional counterfactual explanations, where the goal is to generate a counterfactual distribution that both remains close to the factual input distribution and achieves a desired shift in model outcomes.

Distributional Counterfactual Explanations (DCE) provides an elegant formulation of this problem using optimal transport [You et al. \(2025\)](#). DCE balances an input-side transport cost that preserves plausibility with an output-side transport cost that enforces target predictions, together with statistical certification via chance-constrained bounds. This distributional perspective offers a principled alternative to instance-level recourse by explicitly reasoning about population structure and group-level feasibility.

Despite its appeal, the practical adoption of DCE solver remains limited by its optimization machinery. This gradient-based algorithm relies on differentiability assumptions and computation graphs, which restrict its applicability to smooth predictive models. While gradient-based optimization is well supported for differentiable models [Glorot et al. \(2011\)](#); [Baydin](#)

et al. (2018), practical tabular systems are often non-differentiable or black-box systems, including tree ensembles, rule-based preprocessing, and mixed discrete-continuous feature constraints Breiman (2001); Friedman (2001); Shwartz-Ziv and Armon (2022); Erickson et al. (2025). In such settings, gradient-driven distributional optimization becomes unreliable or infeasible.

More importantly, simply replacing gradients with random sampling is not sufficient. Distributional counterfactual generation is a highly non-convex problem over mixed-type spaces, where naive derivative-free search can be prohibitively inefficient and unstable at the population scale. This motivates the need for a solver that is model-agnostic while still exploiting the structure of optimal transport objectives.

1.2 Main Contributions

In this work, we propose **DISCOVER**, a model-agnostic solver for distributional counterfactual explanations that preserves the certified DCE objective while rethinking the optimization paradigm. Our key insight is that optimal transport based distributional objectives admit a practical sample-level structure: global transport shifts can often be attributed to a small subset of influential samples. A comparison of existing counterfactual paradigms and their properties is summarized in Table 1.

DISCOVER operationalizes this insight through per-sample impact scoring and a top- k budget that localizes and edits the most influential individuals, yielding a sparse and interpretable form of distribution-level intervention.

Building on this structure, DISCOVER formulates distributional counterfactual generation as an iterative propose-and-select search over candidate counterfactual distributions, where multiple candidate updates are generated and the candidate minimizing the certified DCE objective is selected.

DISCOVER further improves black-box search by introducing an input-side OT guidance primitive that exploits the geometry induced by the input-side transport discrepancy to steer proposals toward high-plausibility regions without querying predictor gradients.

- *Sparse Distributional Editing via OT Decomposition:* We reformulate the distributional alignment problem by uncovering a sample-wise decomposition of the OT objective. This allows us to introduce a top- k impact budget, localizing interventions to the most influential samples for sparse and interpretable

updates.

- *Modular Propose-and-Select Architecture:* We propose a solver-agnostic framework that separates candidate generation from objective certification. This design enables certified distributional counterfactual generation in non-smooth and mixed-type spaces where traditional gradient-based methods fail.
- *Predictor-Gradient-Free Geometric Guidance:* We introduce an OT-guided cone sampling primitive that leverages input-side transport gradients. This mechanism provides directed, geometry-aware proposals for black-box models, significantly improving search efficiency over naive derivative-free methods.
- *Unified Solution for Black-Box Pipelines:* We demonstrate that DISCOVER achieves strong joint alignment of input and output distributions across differentiable as well as non-differentiable predictors, effectively extending certified distributional reasoning to modern tabular pipelines.

2 Distributional Counterfactual Formulation and Limitations

Here we briefly review the distributional counterfactual formulation introduced by DCE to establish notation and certification semantics. We then describe the combined objective used to operationalize the chance constraints, before discussing why the original gradient-based optimization becomes problematic in realistic tabular pipelines. This sets the stage for the solver redesign introduced in the next section.

2.1 Problem Formulation

Let $b : \mathcal{R}^d \rightarrow \mathcal{R}$ be a black-box model. Given a factual input distribution \mathbf{x}' with outputs $y' = b(\mathbf{x}')$ and a target output distribution y^* , DCE seeks a counterfactual input distribution \mathbf{x} that remains close to \mathbf{x}' while aligning the model output distribution $b(\mathbf{x})$ with y^* . The problem is formulated over empirical samples and enforces robustness through chance constraints on both the input and output sides.

To measure input proximity, DCE employs the sliced Wasserstein distance \mathcal{SW}^2 , which remains scalable in high dimensions, while output alignment is measured using the Wasserstein distance \mathcal{W}^2 , capturing discrepancies at the distributional level rather than only in expectation You et al. (2025).

Table 1: Comparison of counterfactual paradigms. DISCOVER keeps DCE’s distribution-level objective and certification, while enabling model-agnostic optimization with explicit top- k budgeted editing.

Method	Dist. goal	Certified	Model-Agnostic	Top- k
Instance CE	No	No	Often Yes	No
Group/Global CE	Partial	No	No	No
DCE You et al. (2025)	Yes	Yes	No	No
DISCOVER (ours)	Yes	Yes	Yes	Yes

$$[\text{DCE Problem}] \quad \max_{\mathbf{x}, P} P \quad (1)$$

$$\text{s.t.} \quad P \leq \mathbb{P}[\mathcal{SW}^2(\mathbf{x}, \mathbf{x}') < U_x] \quad (2)$$

$$P \leq \mathbb{P}[\mathcal{W}^2(b(\mathbf{x}), y^*) < U_y] \quad (3)$$

$$P \geq 1 - \frac{\alpha}{2}. \quad (4)$$

Constraint equation 2 enforces proximity between the candidate and factual input distributions, while equation 3 imposes the analogous requirement on the model outputs relative to y^* . The confidence level α in equation 4 guarantees joint satisfaction of both constraints with probability at least $1 - \alpha/2$. This chance-constrained optimal-transport formulation provides interpretable, distribution-level alignment while remaining scalable to high-dimensional inputs via slicing.

2.2 Distributional Counterfactual Objective

Building on the formulation above, let Q_x and Q_y denote the input-side and output-side transport costs induced by sliced Wasserstein and Wasserstein distances, respectively. To operationalize the chance-constrained problem, DCE combines these two costs through an objective with a trade-off parameter $\eta \in [0, 1]$,

$$Q(x, \mu, \nu, \eta) \triangleq (1 - \eta) Q_x(x, \mu) + \eta Q_y(x, \nu), \quad (5)$$

where μ and ν denote the corresponding optimal transport plans. For suitable choices of η , minimizing Q yields candidate solutions that satisfy the empirical chance constraints in equation 2–equation 4 with high probability, highlighting the role of balancing input proximity and output alignment.

2.3 Limitations of Gradient-Based Optimization

Tabular prediction tasks often rely on non-differentiable or only piecewise smooth models [Shwartz-Ziv and Armon \(2022\)](#); [Erickson et al. \(2025\)](#). Tree- and rule-based methods remain strong baselines in this setting, particularly for datasets with mixed

feature types, missing values, and structured constraints [Breiman \(2001\)](#); [Friedman \(2001\)](#). Moreover, real-world tabular pipelines frequently include pre-processing steps such as discretization, thresholding, and rule-based logic, which can render an otherwise differentiable model non-differentiable as a whole. As a result, many deployed tabular systems do not provide reliable input gradients.

However, the limitations of gradient-based solvers in distributional counterfactual generation extend beyond the mere absence of gradients. The original DCE solver performs joint updates of an empirical counterfactual distribution through smooth descent steps, implicitly assuming that the optimization landscape is well behaved under global, population-wide perturbations. In realistic tabular settings, the distributional objective is highly non-convex and defined over mixed continuous and categorical domains, where gradients can be unstable, noisy, or misleading even when differentiability holds.

More fundamentally, optimal-transport-based distributional objectives exhibit an inherent sample-wise coupling structure: population level shifts are often driven by a relatively small subset of influential individuals rather than uniform movement of all samples. This suggests that practical recourse interventions are naturally budgeted, in the sense that only a limited number of instances can be meaningfully edited at each step while the remainder of the empirical distribution should remain unchanged. Gradient-based solvers, which treat all samples symmetrically, fail to exploit this sparsity and can therefore produce inefficient or difficult-to-interpret updates.

These challenges motivate the need for a model-agnostic optimization paradigm that (i) localizes distribution editing under an explicit top- k intervention budget, and (ii) enables structured search over counterfactual distributions without relying on predictive model gradients, while preserving the certified DCE objective.

3 DISCOVER: OT-Structured Sparse Distributional Search

DISCOVER is a solver for Distributional Counterfactual Explanations that preserves the DCE objective and certification layer, while introducing an OT-structured optimization paradigm for black-box and mixed-type tabular pipelines. Instead of treating distribution editing as a global gradient descent over all samples, DISCOVER explicitly exploits the sample-wise structure induced by optimal transport. It performs budgeted sparse distribution editing via top- k impact selection, and optimizes the certified objective through a propose-and-select search over candidate counterfactual distributions. All candidate distributions are evaluated by the same distribution-level objective Q with the same certification mechanism as DCE. DISCOVER does not require gradients of the predictive model.

3.1 DISCOVER framework

At each iteration, DISCOVER first evaluates the current distribution using the same sliced Wasserstein distance on inputs and one-dimensional Wasserstein distance on outputs as in DCE. These distances are computed from empirical optimal transport plans and certified using the same trimmed quantile bands and upper-confidence limits. The balance parameter η is updated using the same interval-narrowing rule. Therefore, DISCOVER changes neither the distributional objective nor the certification semantics.

The optimization challenge in tabular settings is not only the lack of model gradients, but also the need for budgeted interventions at the population level. DISCOVER makes this budget explicit. It attributes the distribution-level objective to sample-wise contributions and edits only a limited subset of influential instances in each iteration.

To operationalize this idea, DISCOVER decomposes the distributional objective into per-row impact scores. On the input side, DCE induces OT plans over one-dimensional projections $\Theta = \{\theta_k\}_{k=1}^N \subset \mathbb{S}^{d-1}$. Under this plan, the input-side contribution of each sample x_i can be written as

$$q_i^{(x)} = \frac{1}{N} \sum_{k=1}^n \sum_{j=1}^n |\theta_k^\top x_i - \theta_k^\top x_j'|^2 \mu_{ij}^{(k)}, \quad (6)$$

which measures how strongly x_i contributes to the current input-side transport discrepancy. An analogous decomposition holds on the output side under the transport plan ν , yielding

$$q_i^{(y)} = \sum_{j=1}^n |b(x_i) - y_j^*|^2 \nu_{ij}. \quad (7)$$

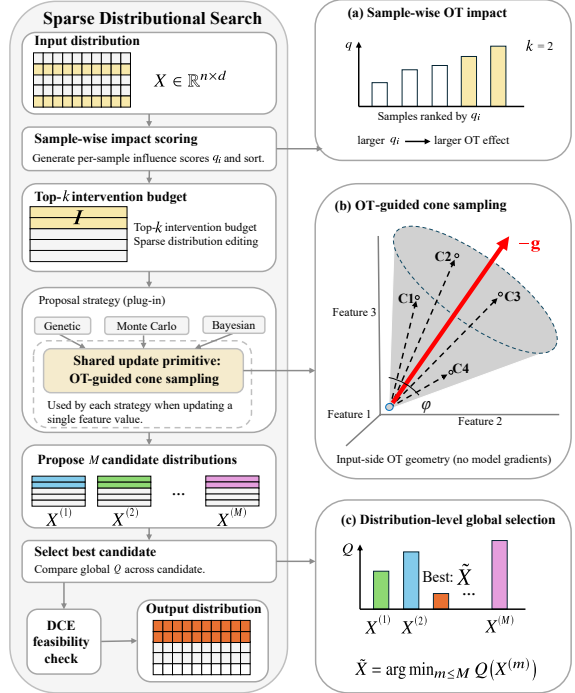


Figure 1: Overview of DISCOVER. DISCOVER preserves the DCE objective Q and its certification layer. At each iteration it computes per-sample impact scores $\{q_i\}$ derived from the current OT-based objective, and selects a top- k active set that defines an explicit intervention budget. It then generates M candidate counterfactual distributions by editing only the selected samples using a shared OT-guided cone sampling primitive. Among the M candidates, DISCOVER selects the one with the smallest certified objective value Q and repeats until the iteration budget is exhausted.

Combining both terms, the overall per-row impact score is defined as

$$q_i = (1 - \eta) q_i^{(x)} + \eta q_i^{(y)}. \quad (8)$$

Proposition 3.1 (Row-wise decomposition of the certified objective). *For fixed OT plans $\mu = \{\mu^{(k)}\}_{k=1}^N$ and ν , the certified objective admits an exact row-wise decomposition $Q(x, \mu, \nu, \eta) = \sum_{i=1}^n q_i$, where $q_i^{(x)}$, $q_i^{(y)}$, and q_i are defined above. In particular, $Q_x(x, \mu) = \sum_{i=1}^n q_i^{(x)}$ and $Q_y(x, \nu) = \sum_{i=1}^n q_i^{(y)}$.*

Proof is provided in Appendix C.

The combined score q_i directly measures how strongly sample x_i contributes to the current certified objective. DISCOVER uses q_i to define a top- k editable set I at each iteration. Only rows in I may change,

Algorithm 1 DISCOVER: Budgeted Propose-and-Select Distributional Solver

Require: Factual sample X' , predictor $b(\cdot)$, target outputs Y^* , bounds (U_x, U_y) , confidence level α , top- k budget k , candidates per iteration M , max iterations T

Ensure: Edited sample \hat{X} or \emptyset

- 1: Initialize $X \leftarrow X'$
 - 2: **for** $t = 1$ to T **do**
 - 3: Evaluate $Q(X; \eta)$ and update η using the same certification and interval-narrowing rule as DCE
 - 4: Compute per-row impact scores $\{q_i\}_{i=1}^n$
 - 5: Select editable row set $I \leftarrow$ indices of the top- k scores
 - 6: Compute input-side OT guidance signal g from $\mathcal{SW}^2(X, X')$
 - 7: Set baseline candidate $X^{(0)} \leftarrow X$ (no-op update)
 - 8: **for** $m = 1$ to M **do**
 - 9: OPTIMIZER (Sec. 3.2) proposes $X^{(m)}$ by editing rows in I using the shared OT-guided cone sampling primitive (Sec.3.3) guided by $-g$
 - 10: **end for**
 - 11: $\hat{X} \leftarrow \arg \min_{m \in \{0, 1, \dots, M\}} Q(X^{(m)}; \eta)$
 - 12: $X \leftarrow \hat{X}$
 - 13: **end for**
 - 14: Check whether \hat{X} satisfies the same DCE certification criteria
 - 15: **if** certification holds **then**
 - 16: **return** \hat{X}
 - 17: **else**
 - 18: **return** \emptyset
 - 19: **end if**
-

and all other rows remain fixed. This top- k gate implements an explicit intervention budget. It reduces the effective search space, improves stability, and yields sparse and interpretable population-level edits, while keeping the objective unchanged.

Given the editable set I , DISCOVER performs a distribution-level propose-and-select search. It generates M candidate counterfactual distributions by editing only rows in I with a shared proposal primitive. Each candidate is evaluated by the same certified objective $Q(\cdot; \eta)$, and the best candidate is selected as the next iterate. We additionally include the current distribution as a baseline no-op candidate (Algorithm 1), which guarantees that the certified objective does not increase within each iteration.

Proposition 3.2 (Monotonicity of the propose-and-s-

elect step). *Let X be the current iterate and let*

$$\hat{X} = \arg \min_{m \in \{0, 1, \dots, M\}} Q(X^{(m)}; \eta)$$

be the selected candidate, where $X^{(0)} = X$ is the no-op proposal and η is fixed during the candidate evaluation. Then $Q(\hat{X}; \eta) \leq Q(X; \eta)$.

Proof is provided in Appendix C.

This explicit candidate selection is a key difference from single-path descent methods and is well-suited for non-convex and mixed-type optimization landscapes.

To bias proposals toward low input distortion without querying predictive model gradients, DISCOVER computes an input-side OT guidance field from $\mathcal{SW}^2(X, X')$ and uses it only in the proposal step. The output side remains fully black-box because no ∇b is required. After the iteration budget, DISCOVER returns the best candidate that satisfies the same DCE certification criteria.

3.2 A Modular Proposal Mechanism for Distributional Search

DISCOVER separates the certified distributional objective from the mechanism that proposes candidate distributions. The modular optimizer is a proposal layer. It receives the current iterate X , the editable row set I induced by the top- k intervention budget, and a small set of exploration parameters. It outputs M candidate distributions $\{X^{(m)}\}_{m=1}^M$ that only edit rows in I and satisfy domain constraints and actionability rules. All optimizers share a common proposal primitive, OT-guided cone sampling (Sec. 3.3), and differ only in how they combine and apply it to generate candidates.

Different optimizers differ only in how they propose candidates. All candidates are evaluated by the same certified objective $Q(\cdot; \eta)$, and DISCOVER selects the best candidate. This makes the overall solver strategy-agnostic while keeping a single objective and a single certification protocol.

Monte Carlo Optimizer. The Monte Carlo optimizer proposes M validity-preserving candidate edits around the current iterate. The top- k gate confines changes to the most influential rows, and an input-side OT guidance field $g = \nabla_X \mathcal{SW}^2(X, X')$ biases proposal directions. Numerical features are perturbed within valid ranges, and categorical features are modified within admissible levels. Among the M candidates, DISCOVER selects the one with the smallest certified objective value.

Genetic Optimizer. The genetic optimizer produces candidates through recombination and guided mutation on the same editable set I . Crossover reuses partial structures from the current iterate, while mutations introduce local variations in a domain-preserving manner. Both operations are biased by the same input-side guidance field g . Each candidate is evaluated by $Q(\cdot; \eta)$, and DISCOVER selects the best candidate.

3.3 OT-Guided Cone Sampling Primitive

Edits are restricted to the current top- k rows I , so that each iteration focuses on the samples under the intervention budget. To guide candidate generation without relying on model gradients, DISCOVER computes a single input-side guidance field

$$-g = -\nabla_x \mathcal{SW}^2(x, x'),$$

which depends only on the sliced Wasserstein distance between the current distribution and the factual reference. This field captures geometry of input-side transport under the current OT structure. It is independent of the predictive model, and ∇b is never queried.

The guidance field g is used only to bias proposal directions. Candidate updates are sampled within a cone of half-angle ϕ around the direction $-g$, take bounded steps, and are projected back to the valid domain. No gradient descent is performed on the full objective Q , and ∇b is never queried. The guidance field is evaluated once per outer iteration and reused across all M candidate trials generated by the modular optimizer, ensuring low overhead while maintaining consistent directional bias.

Algorithm 2 OT-guided cone sampling for numerical features

- 1: **Input:** row index i , current row x_i , editable indices \mathcal{R} , guidance g , feature ranges $\{\{R_p^{\min}, R_p^{\max}\}\}_{p \in \mathcal{R}}$
 - 2: **Output:** updated row x_i on \mathcal{R}
 - 3: **for** $p \in \mathcal{R}$ **do**
 - 4: sample direction d_{ip} in a cone around $-g$ (half-angle ϕ)
 - 5: sample a step size $\lambda \in [0, \lambda_{\max}]$
 - 6: update $x_{ip} \leftarrow \Pi_{[R_p^{\min}, R_p^{\max}]}(x_{ip} + \lambda(R_p^{\max} - R_p^{\min})d_{ip})$
 - 7: **end for**
 - 8: **return** updated x_i .
-

Numerical coordinates. For numerical features, DISCOVER generates proposals using a shared OT-guided cone sampling primitive. Each editable row

is updated by sampling a direction that is biased toward the negative input-side guidance field $-g$, where $g = \nabla_x \mathcal{SW}^2(X, X')$ depends on the transport discrepancy to the factual distribution. This provides a lightweight geometric prior that favors low-distortion edits in the input space, without requiring any gradient information from the predictive model.

The cone half-angle ϕ controls the concentration of proposals around this OT-induced direction, interpolating between focused transport-consistent moves and broader exploration. A bounded step size $\lambda \in [0, \lambda_{\max}]$ is drawn and scaled by the feature range $(R_p^{\max} - R_p^{\min})$ to normalize updates across heterogeneous units. Each proposed update is finally projected onto the valid interval $[R_p^{\min}, R_p^{\max}]$, ensuring feasibility by construction. This procedure yields numerical candidate distributions that preserve input-side plausibility while enabling effective distribution-level search under the top- k intervention budget.

Algorithm 3 OT-guided cone sampling for categorical features

- 1: **Input:** row index i , current row x_i , editable indices \mathcal{C} , guidance g , temperature τ
 - 2: **Output:** updated row x_i on \mathcal{C}
 - 3: **for** $p \in \mathcal{C}$ **do**
 - 4: represent category x_{ip} as a one-hot vector $o_{ip} \in \{0, 1\}^{|\mathcal{V}_p|}$
 - 5: embed $z_{ip} \leftarrow E_p[x_{ip}]$ where $E_p \in \mathbb{R}^{|\mathcal{V}_p| \times r}$ is a fixed embedding table (initialized once and kept constant)
 - 6: take a cone-biased embedding step: $\tilde{z}_{ip} \leftarrow z_{ip} + \Delta$, where $\Delta \in \mathbb{R}^r$ is sampled in a cone around $-g$ (half-angle ϕ)
 - 7: include the no-op option $v = x_{ip}$ in the admissible set under actionability constraints
 - 8: decode by sampling a category with $\Pr(v) \propto \exp(-\|E_p[v] - \tilde{z}_{ip}\|^2/\tau)$ under actionability constraints
 - 9: **end for**
 - 10: **return** updated x_i .
-

Categorical coordinates. For categorical features, DISCOVER performs proposals in a numerical embedding space where directions are meaningful. For each categorical feature p , we construct a fixed embedding table $E_p \in \mathbb{R}^{|\mathcal{V}_p| \times r}$ once before optimization and keep it constant throughout. In our implementation, E_p is randomly initialized with a fixed random state for reproducibility, and r is chosen by a deterministic rule based on the category cardinality $|\mathcal{V}_p|$ unless specified. A cone-biased step guided by $-g$ is then applied in the embedding space. To decode

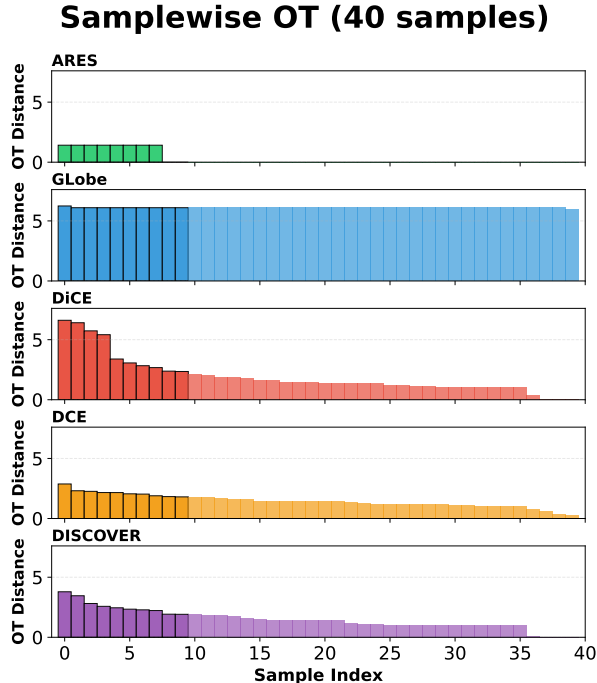


Figure 2: Per-sample input-side OT distances on COMPAS with an MLP. Distances are sorted in descending order within each method, highlighting the top-10 largest values. All methods share the same y-axis scale for fair comparison.

back to a discrete category, we compute distances between the updated embedding and all category embeddings and sample with a temperature-controlled rule. Specifically, the probability of category v is proportional to $\exp(-\|E_p[v] - \tilde{z}\|^2/\tau)$, where $E_p[v] \in \mathbb{R}^r$ denotes the embedding vector of category v . The temperature τ controls the exploration and exploitation trade-off. Finally, decoding is restricted to admissible categories under predefined domain and actionability constraints.

4 Experimental Setup and Results

4.1 Experimental Setup

We evaluate DISCOVER mainly on five tabular datasets: HELOC FICO (2018), COMPAS Larson et al. (2016), Hotel Booking Antonio et al. (2019), German Credit Hofmann (1994), and Cardiovascular Disease Halder (2020). Quantitative comparisons are performed on HELOC, COMPAS and German Credit, where DISCOVER is compared with existing CE methods, including DCE You et al. (2025), DiCE Mothilal et al. (2020), AReS Rawal and Lakkaraju (2020), and GLOBE Ley et al. (2023). DiCE generates counterfactuals independently for individual instances, whereas AReS and GLOBE

Empirical CDF Comparison (Y)

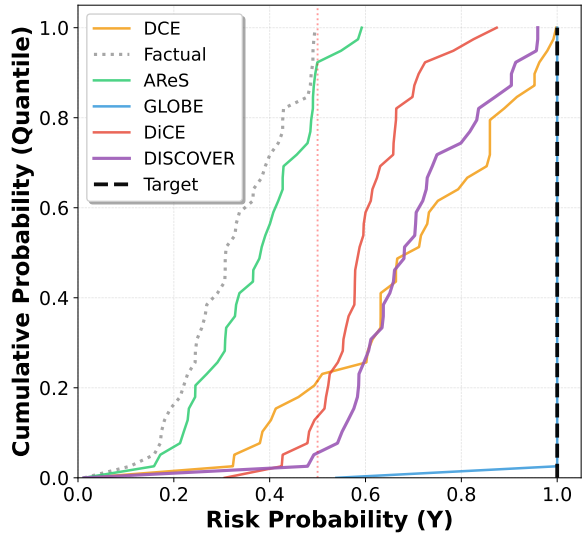


Figure 3: Empirical CDFs of model output distributions on COMPAS with an MLP. Shown are the factual outputs, the target distribution, and counterfactual outputs produced by different methods.

operate at the group level by aggregating recourse patterns across samples. DCE is included as a gradient-based baseline in settings where differentiability is available, enabling a direct comparison between gradient-based optimization and the proposed model-agnostic solver under the same distributional objectives.

The main evaluation targets the distributional alignment objective inherited from DCE. We primarily report $OT(x)$ and $OT(y)$, which quantify input-side plausibility preservation and output-side target attainment, respectively. We also report MMD and AReS Cost to match prior evaluation protocols. Ablation test the necessity of DISCOVER’s solver components: (i) sample-wise OT impact scoring and the top- k intervention budget, (ii) propose-and-select candidate search over multiple proposals per iteration, and (iii) OT-guided cone sampling as a shared proposal primitive. Extended results and additional settings are reported in the Appendix D and E.

4.2 Main Results

Figures 2 and 3 provide a qualitative comparison of input distortion and output shift across methods. Conservative methods can preserve the input distribution while failing to induce a meaningful output shift. AReS produces uniformly small per-sample input-side transport distances, but its output CDF remains close to the factual distribution, leading to

Table 2: Comparison of DISCOVER with CE baselines on tabular datasets. We report Diff. and Non-diff. models. $OT(x)/OT(y)$ are input/output Wasserstein distances and our primary distributional criteria (lower is better). AReS Cost is reported for reference only (not optimized by DISCOVER). DCE is included only in Diff. settings. Results are mean \pm 80% CI over SVM, MLP, RF, XGBoost, and LightGBM. Gray entries are excluded; bold denotes best among remaining methods.

Dataset	Method	$OT(x)$	$OT(y)$	MMD	AReS Cost
COMPAS (Diff.)	AReS	0.0222 \pm 0.0566	0.5389 \pm 0.0425	0.0261 \pm 0.0713	2.0764 \pm 2.0380
	GLOBE	20.5166 \pm 53.6786	0.0088 \pm 0.0271	0.2422 \pm 0.0499	1.0703 \pm 1.8080
	DiCE	0.1124 \pm 0.0863	0.2273 \pm 0.0505	0.0553 \pm 0.0129	3.9354 \pm 0.0057
	DCE	0.0930 \pm 0.0220	0.1576 \pm 0.0300	0.0894 \pm 0.0211	4.0677 \pm 1.1666
	DISCOVER	0.0681 \pm 0.0252	0.1474 \pm 0.0576	0.0679 \pm 0.0203	4.0370 \pm 0.6362
COMPAS (Non-diff.)	AReS	0.0174 \pm 0.0195	0.4990 \pm 0.1350	0.0281 \pm 0.0349	0.9278 \pm 0.8920
	GLOBE	0.3537 \pm 0.0275	0.2480 \pm 0.0166	0.2031 \pm 0.0258	1.4250 \pm 0.8522
	DiCE	0.0673 \pm 0.0045	0.2376 \pm 0.0329	0.0867 \pm 0.0064	2.2813 \pm 0.4523
	DCE	-	-	-	-
	DISCOVER	0.0586 \pm 0.0021	0.1412 \pm 0.0473	0.0838 \pm 0.0103	2.9224 \pm 0.0981
HELOC (Diff.)	AReS	0.0005 \pm 0.0005	0.2956 \pm 0.0045	0.0003 \pm 0.0003	1.7751 \pm 4.8569
	GLOBE	1.5997 \pm 0.2901	0.1166 \pm 0.0302	0.0060 \pm 0.0003	2.5810 \pm 0.0673
	DiCE	0.0218 \pm 0.0180	0.1641 \pm 0.0606	0.0054 \pm 0.0003	5.5336 \pm 5.1293
	DCE	0.1196 \pm 0.1408	0.1381 \pm 0.1074	0.0152 \pm 0.0069	6.3231 \pm 0.2319
	DISCOVER	0.0139 \pm 0.0112	0.1897 \pm 0.0245	0.0033 \pm 0.0021	9.4846 \pm 0.1944
HELOC (Non-diff.)	AReS	0.0008 \pm 0.0002	0.5184 \pm 0.1966	0.0007 \pm 0.0002	0.0738 \pm 0.0043
	GLOBE	6.6634 \pm 5.5036	0.1138 \pm 0.0823	0.0602 \pm 0.0507	2.5813 \pm 0.1247
	DiCE	0.0704 \pm 0.0412	0.2315 \pm 0.0423	0.0455 \pm 0.0371	3.9318 \pm 2.0387
	DCE	-	-	-	-
	DISCOVER	0.0514 \pm 0.0479	0.1595 \pm 0.0353	0.0320 \pm 0.0264	3.9616 \pm 1.9334
German Credit (Diff.)	AReS	0.0182 \pm 0.0548	0.7827 \pm 1.2471	0.0306 \pm 0.0891	0.8536 \pm 0.4507
	GLOBE	230.8465 \pm 468.6101	0.0082 \pm 0.0252	0.2499 \pm 0.5466	0.2164 \pm 0.0719
	DiCE	0.0552 \pm 0.1437	0.1101 \pm 0.2879	0.1196 \pm 0.2364	4.5631 \pm 10.1682
	DCE	0.0213 \pm 0.0234	0.5214 \pm 0.4393	0.0324 \pm 0.0131	5.8666 \pm 17.4976
	DISCOVER	0.0465 \pm 0.1253	0.1025 \pm 0.0922	0.0969 \pm 0.1988	2.8578 \pm 4.1513
German Credit (Non-diff.)	AReS	0.0029 \pm 0.0030	0.6675 \pm 0.2290	0.0079 \pm 0.0068	1.1267 \pm 1.1450
	GLOBE	0.0300 \pm 0.0046	0.3609 \pm 0.0041	0.0519 \pm 0.0135	0.9147 \pm 0.1440
	DiCE	0.0124 \pm 0.0083	0.3636 \pm 0.1834	0.0468 \pm 0.0304	5.0579 \pm 0.7173
	DCE	-	-	-	-
	DISCOVER	0.0117 \pm 0.0070	0.2285 \pm 0.0528	0.0470 \pm 0.0323	6.9458 \pm 1.7376

large $OT(y)$.

In contrast, aggressive group-level translations can match the target outputs while severely distorting inputs. GLOBE aligns the output distribution closely to the target, but does so with substantially larger per-sample $OT(x)$, indicating global distortion.

DISCOVER achieves a sparse and coordinated intervention pattern. It concentrates edits on a small subset of influential samples, yielding a controlled $OT(x)$ profile while producing an output CDF that closely tracks the target. This supports the motivation behind budgeted sparse distribution editing: effective distributional explanations require selective, coordinated edits rather than uniformly small or uniformly large changes.

We report the main quantitative comparison in Table 2. Results are averaged over five predictive models (SVM, MLP, Random Forest, XGBoost, and LightGBM) and are reported separately for differentiable and non-differentiable settings.

We focus primarily on $OT(x)$ and $OT(y)$, which respectively measure the Wasserstein distance between the factual and counterfactual input and output distributions. These metrics directly reflect the quality of distributional counterfactual explanations, as they assess whether counterfactual edits simultaneously preserve the structure of the input distribution while steering model predictions toward the desired target distribution.

Across datasets, DISCOVER attains the best or second-best $OT(x)$ in most settings and achieves the lowest $OT(y)$ in all non differentiable settings.

In contrast, several baseline methods exhibit imbalanced behavior between $OT(x)$ and $OT(y)$. For instance, AReS frequently attains extremely small $OT(x)$ and MMD values, suggesting minimal perturbations to the input distribution. However, this behavior is accompanied by substantially larger $OT(y)$ values in nearly all cases, showing that the output distribution remains far from the target. This reflects the rule-based nature of AReS, which prioritizes

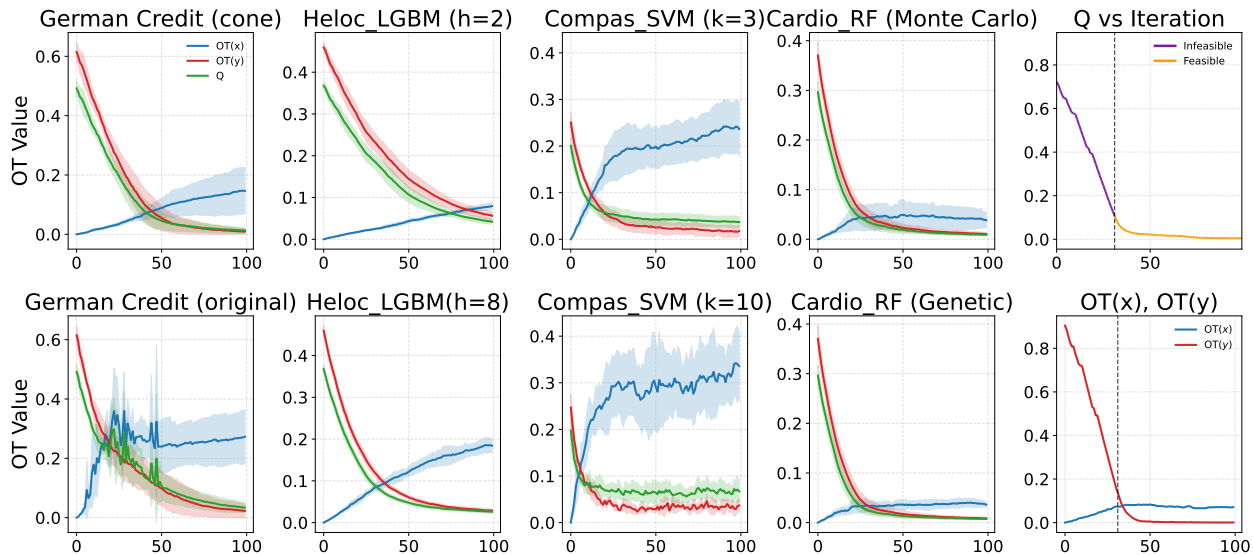


Figure 4: Optimization dynamics of DISCOVER across datasets and model architectures. Each subplot shows $OT(x)$, $OT(y)$, and the objective Q over iterations. $OT(x)$ (blue) measures input-side Wasserstein distance, and $OT(y)$ (orange) measures output-side distance to the target. Solid lines denote the mean over five random seeds, with shaded regions indicating standard deviation. Results show stable and consistent convergence across datasets, models, and solver settings.

conservative feature edits and feasibility constraints, often at the expense of achieving meaningful distributional shifts in model predictions. This leads to counterfactual distributions that remain close to the factual outputs under the OT criterion.

Similarly, DiCE, as an instance-based method, struggles to coordinate counterfactual edits across samples. While it may achieve reasonable $OT(x)$ values in some settings, its $OT(y)$ values are consistently higher than those of DISCOVER, indicating limited ability to align output distributions at the group level. This is consistent with the limitation of instance-wise generation when the evaluation target is defined over distributions.

GLOBE exhibits high variance and occasionally extremely large $OT(x)$ values (e.g., German Credit), while achieving very small $OT(y)$. This indicates that GLOBE can reach output alignment by applying large, near-uniform translations across many samples, which moves the empirical input distribution far from the factual manifold. Because $OT(x)$ is a distribution-level transport distance, a small number of failed or overly aggressive runs can dominate the mean and inflate the confidence interval. We therefore interpret these results as evidence that translation-based group recourse can be unstable under mixed constraints, and we complement mean statistics with per-sample profiles in Figure 2.

The original DCE method is included as a baseline in differentiable settings. Although DCE and DISCOVER optimize the same certified distributional objective, DISCOVER remains competitive with DCE and can sometimes achieve lower $OT(x)/OT(y)$ under the same evaluation budget. We attribute this behavior to the solver paradigm rather than a change of objective. DCE follows a single-path gradient descent that updates all samples simultaneously, which can be sensitive to non-convexity, slicing approximations, and mixed-type constraints. In contrast, DISCOVER performs budgeted sparse edits and applies a propose-and-select search over multiple candidate distributions, providing a more robust update mechanism under stochastic and discrete proposal dynamics. Consistent with this explanation, Figure 4 shows that OT-guided proposals stabilize optimization trajectories, while overly aggressive population updates (larger k) lead to unstable behavior. Additional ablations on key solver components are reported in the Appendix D.

4.3 Ablation Study

We ablate solver components (Figure 4) and editable feature subsets (Table 3), and sweep h and k to study stability–efficiency trade-offs under a fixed evaluation budget.

Table 3 shows that allowing both numerical and categorical edits generally yields the lowest $OT(x)$. Re-

Table 3: Ablation of editable feature subsets. Results are averaged over models (treated as independent runs) and reported as mean \pm 95% confidence interval. For each dataset, the best (lowest) value for each metric is highlighted in bold.

Dataset	Method	OT(x)	OT(y)	MMD	ARes Cost
COMPAS	DISCOVER	0.112800 \pm 0.038690	0.028067 \pm 0.007056	0.046067 \pm 0.012027	8.643200 \pm 0.813492
	Categorical only	0.142267 \pm 0.041301	0.029733 \pm 0.006039	0.049400 \pm 0.010146	8.800867 \pm 0.864495
	numerical only	0.118333 \pm 0.039038	0.024933 \pm 0.006147	0.046867 \pm 0.010116	8.742867 \pm 0.669316
	No editing	0.140867 \pm 0.040595	0.028533 \pm 0.005470	0.049667 \pm 0.008073	9.123267 \pm 0.613175
Cardio	DISCOVER	0.052900 \pm 0.008728	0.019350 \pm 0.002854	0.022300 \pm 0.001457	7.216050 \pm 0.461864
	Categorical only	0.076800 \pm 0.018989	0.014000 \pm 0.003957	0.026750 \pm 0.001730	7.447850 \pm 0.497926
	numerical only	0.065000 \pm 0.008903	0.020600 \pm 0.003084	0.027950 \pm 0.001596	8.578950 \pm 0.454685
	No editing	0.090850 \pm 0.018019	0.015500 \pm 0.003870	0.032600 \pm 0.002106	8.797000 \pm 0.543489
HELOC	DISCOVER	0.096000 \pm 0.015814	0.059650 \pm 0.017533	0.027950 \pm 0.001819	7.748600 \pm 0.622564
	Categorical only	0.149000 \pm 0.022498	0.059950 \pm 0.018815	0.029500 \pm 0.001863	8.817000 \pm 0.804573
	numerical only	0.109700 \pm 0.018299	0.056550 \pm 0.017828	0.029150 \pm 0.001651	8.196950 \pm 1.058611
	No editing	0.160500 \pm 0.025151	0.057250 \pm 0.018835	0.029500 \pm 0.001639	9.648950 \pm 0.817946
German Credit	DISCOVER	0.112600 \pm 0.015718	0.043000 \pm 0.024616	0.033900 \pm 0.002087	7.534250 \pm 0.273088
	Categorical only	0.189250 \pm 0.033634	0.048850 \pm 0.026457	0.035700 \pm 0.001692	7.282100 \pm 0.237567
	numerical only	0.103700 \pm 0.015955	0.040800 \pm 0.024742	0.035300 \pm 0.001860	8.544250 \pm 0.341697
	No editing	0.163100 \pm 0.024923	0.041900 \pm 0.025018	0.037700 \pm 0.001758	8.369600 \pm 0.267596
Hotel Booking	DISCOVER	0.108120 \pm 0.022602	0.025680 \pm 0.009189	0.025880 \pm 0.001285	16.480120 \pm 2.742385
	Categorical only	0.193640 \pm 0.073230	0.034840 \pm 0.016852	0.025960 \pm 0.001302	18.282440 \pm 3.372114
	numerical only	0.124960 \pm 0.027583	0.019200 \pm 0.007702	0.027040 \pm 0.001324	15.646160 \pm 2.546458
	No editing	0.177160 \pm 0.050751	0.029120 \pm 0.015467	0.027000 \pm 0.001294	18.604800 \pm 3.164555

stricting edits to a single type often increases $OT(x)$, indicating reduced flexibility for transport-consistent low-distortion updates.

For $OT(y)$, numerical-only editing is often competitive (e.g., COMPAS, HELOC, German Credit, and Hotel Booking), while categorical edits matter on datasets where discrete switches are needed (e.g., Cardio). Overall, enabling both types provides the most reliable balance between $OT(x)$ and $OT(y)$. This is consistent with the objective structure: numerical edits follow the continuous geometry of \mathcal{SW}^2 , whereas categorical edits introduce discrete moves that can be harder to optimize but sometimes necessary.

Numerical updates align well with the continuous geometry induced by \mathcal{SW}^2 , while categorical updates introduce discrete jumps that can be harder to optimize but may be necessary to achieve target alignment under constraints.

Figure 4 summarizes optimization trajectories of $OT(x)$, $OT(y)$, and Q across datasets, models, and solver settings.

Column 1 compares German Credit under two settings: with OT-guided cone sampling (top) and without it (bottom). When cone guidance is enabled, all three quantities decrease smoothly and remain stable. Without guidance, $OT(x)$ shows large fluctuations, which propagate to the objective Q . As a result, both the final $OT(x)$ and $OT(y)$ values and the objective are worse than in the guided case, highlighting the stabilizing role of input-side geometric guidance.

The second column analyzes the effect of h , the number of features updated per selected sample, on HELOC with LightGBM. Increasing h from 2 to 8 leads to faster convergence. The variance of Q and $OT(y)$ is substantially larger for $h = 2$, while $h = 8$ yields smoother trajectories. Larger h accelerates the decrease of Q and $OT(y)$, at the cost of a modest increase in $OT(x)$ variance.

The third column studies the impact of k , the number of samples updated per iteration, on COMPAS with an SVM. With $k = 3$, $OT(x)$, $OT(y)$, and Q converge smoothly and remain stable. In contrast, $k = 10$ leads to large fluctuations and wide variance bands, and the final solution is inferior across all metrics. This supports the top- k design: sparse interventions stabilize the OT objective, while large- k updates amplify coupling noise.

The fourth column compares Monte Carlo and Genetic optimizers on Cardio with a Random Forest. Both optimizers reach similar mean trajectories and final values of Q . However, Monte Carlo exhibits noticeably larger variance, reflecting higher stochasticity across runs.

The last column visualizes feasibility during optimization. The top panel plots Q , where purple indicates infeasible iterates and yellow indicates feasible ones. After a finite number of iterations, marked by the vertical dashed line, the optimization enters the feasible region. The bottom panel shows that this transition coincides with a balance between $OT(x)$ and $OT(y)$, confirming that feasibility is achieved when input

proximity and output alignment are jointly satisfied.

5 Conclusion

In this paper, we introduced DISCOVER, a model-agnostic solver for distributional counterfactual explanations that preserves the certified optimal-transport objective of DCE. DISCOVER identifies influential samples through a sample-wise OT decomposition and applies a top- k intervention budget to localize distributional edits. Across multiple tabular datasets and predictors, DISCOVER achieves strong alignment between input and output distributions. Crucially, these improvements are obtained without relying on predictive model gradients. As a modular and architecture-agnostic approach, DISCOVER integrates naturally with black-box tabular pipelines and broadens the applicability of certified distributional explanations.

References

- Nuno Antonio, Ana de Almeida, and Luis Nunes. Hotel booking demand datasets. *Data in brief*, 22:41–49, 2019.
- Atilim Gunes Baydin, Barak A Pearlmutter, Alexey Andreyevich Radul, and Jeffrey Mark Siskind. Automatic differentiation in machine learning: a survey. *Journal of machine learning research*, 18(153):1–43, 2018.
- Leo Breiman. Random forests. *Machine learning*, 45(1): 5–32, 2001.
- Susanne Dandl, Kristin Blesch, Timo Freiesleben, Gunnar König, Jan Kapar, Bernd Bischl, and Marvin N Wright. Counterfactuals—generating plausible model-agnostic counterfactual explanations with adversarial random forests. In *World Conference on Explainable Artificial Intelligence*, pages 85–107, 2024.
- Sopam Dasgupta, Sadaf Halim, Joaquín Arias, Elmer Salazar, and Gopal Gupta. Mc3g: Model agnostic causally constrained counterfactual generation. *arXiv preprint arXiv:2508.17221*, 2025.
- Rudresh Dwivedi, Devam Dave, Het Naik, Smiti Singhal, Rana Omer, Pankesh Patel, Bin Qian, Zhenyu Wen, Tejal Shah, Graham Morgan, et al. Explainable ai (xai): Core ideas, techniques, and solutions. *ACM computing surveys*, 55(9):1–33, 2023.
- Nick Erickson, Lennart Purucker, Andrej Tschalzev, David Holzmüller, Prateek Mutalik Desai, David Salinas, and Frank Hutter. Tabarena: A living benchmark for machine learning on tabular data. *arXiv preprint arXiv:2506.16791*, 2025.
- FICO. Fico explainable machine learning challenge, 2018.
- Jerome H Friedman. Greedy function approximation: a gradient boosting machine. *Annals of statistics*, 29(5): 1189–1232, 2001.
- Xavier Glorot, Antoine Bordes, and Yoshua Bengio. Deep sparse rectifier neural networks. In *14th International Conference on Artificial Intelligence and Statistics*, volume 15, pages 315–323, 2011.
- Riccardo Guidotti. Counterfactual explanations and how to find them: Literature review and benchmarking. *Data Mining and Knowledge Discovery*, pages 1–55, 2022.
- R. K. Halder. Cardiovascular disease dataset, 2020.
- Hans Hofmann. Statlog (german credit data), 1994. UCI Machine Learning Repository.
- Amir-Hossein Karimi, Gilles Barthe, Borja Balle, and Isabel Valera. Model-agnostic counterfactual explanations for consequential decisions. In *International conference on artificial intelligence and statistics*, pages 895–905, 2020.
- Jeff Larson, Lauren Kirchner, Surya Mattu, and Julia Angwin. How we analyzed the compas recidivism algorithm, 2016.
- Dan Ley, Saumitra Mishra, and Daniele Magazzeni. Globe-ce: A translation based approach for global counterfactual explanations. In *International conference on machine learning*, pages 19315–19342, 2023.
- Ramaravind K Mothilal, Amit Sharma, and Chenhao Tan. Explaining machine learning classifiers through diverse counterfactual explanations. In *Proceedings of the 2020 conference on fairness, accountability, and transparency*, pages 607–617, 2020.
- Gabriel Peyré, Marco Cuturi, et al. Computational optimal transport: With applications to data science. *Foundations and Trends® in Machine Learning*, 11 (5-6):355–607, 2019.
- Gregory Plumb, Jonathan Terhorst, Sriram Sankararaman, and Ameet Talwalkar. Explaining groups of points in low-dimensional representations. In *International Conference on Machine Learning*, pages 7762–7771, 2020.
- Rafael Poyiadzi, Kacper Sokol, Raul Santos-Rodriguez, Tijn De Bie, and Peter Flach. Face: feasible and actionable counterfactual explanations. In *Proceedings of the AAAI/ACM Conference on AI, Ethics, and Society*, pages 344–350, 2020.
- Kaivalya Rawal and Himabindu Lakkaraju. Beyond individualized recourse: Interpretable and interactive summaries of actionable recourses. *Advances in Neural Information Processing Systems*, 33:12187–12198, 2020.
- Robert-Florian Samoilescu, Arnaud Van Looveren, and Janis Klaise. Model-agnostic and scalable counterfactual explanations via reinforcement learning. *arXiv preprint arXiv:2106.02597*, 2021.
- Ravid Shwartz-Ziv and Amitai Armon. Tabular data:

- Deep learning is not all you need. *Information Fusion*, 81:84–90, 2022.
- Berk Ustun, Alexander Spangher, and Yang Liu. Actionable recourse in linear classification. In *Proceedings of the conference on fairness, accountability, and transparency*, pages 10–19, 2019.
- Sahil Verma, Varich Boonsanong, Minh Hoang, Keegan Hines, John Dickerson, and Chirag Shah. Counterfactual explanations and algorithmic recourses for machine learning: A review. *ACM Computing Surveys*, 56(12): 1–42, 2024.
- Sandra Wachter, Brent Mittelstadt, and Chris Russell. Counterfactual explanations without opening the black box: Automated decisions and the gdpr. *Harv. JL & Tech.*, 31:841, 2017.
- Geemi P Wellawatte, Aditi Seshadri, and Andrew D White. Model agnostic generation of counterfactual explanations for molecules. *Chemical science*, 13(13): 3697–3705, 2022.
- Wenzhuo Yang, Jia Li, Caiming Xiong, and Steven CH Hoi. Mace: An efficient model-agnostic framework for counterfactual explanation. *arXiv preprint arXiv:2205.15540*, 2022.
- Lei You, Lele Cao, Mattias Nilsson, Bo Zhao, and Lei Lei. Distributional counterfactual explanations with optimal transport. In *International Conference on Artificial Intelligence and Statistics*, pages 1135–1143, 2025.
- Lei You, Yijun Bian, and Lele Cao. Joint distribution-informed shapley values for sparse counterfactual explanations. In *The Fourteenth International Conference on Learning Representations*, 2026. URL <https://openreview.net/forum?id=3vIe5pNiUN>.

A Related Work

Counterfactual explanations (CE) aim to provide actionable insight by identifying feasible input changes that alter a model prediction. Wachter et al. Wachter et al. (2017) formulate CE as an optimization problem that balances proximity to the factual instance and alignment with a target outcome, which has motivated a broad literature Guidotti (2022).

Instance-level counterfactuals and recourse. Most existing methods generate counterfactuals for individual instances. They incorporate feasibility constraints, immutable features, and user-defined costs to ensure valid edits Poyiadzi et al. (2020); Ustun et al. (2019); Karimi et al. (2020), and extend this setting to produce diverse counterfactual sets for a single instance Mothilal et al. (2020). These approaches are effective for individual recourse, but their objectives and guarantees are defined at the instance level.

Group-level and global summaries. Recent work also considers cohort-level recourse and global summaries. AReS Rawal and Lakkaraju (2020) summarizes actionable recourse patterns for subpopulations using rule-based representations, while GLOBE Ley et al. (2023) targets scalable global counterfactual summaries. Related methods analyze subgroup-level feature differences or aggregate instance-level edits Plumb et al. (2020). However, these approaches typically summarize sets of instance-wise counterfactuals rather than optimizing a distribution-level objective with explicit statistical certification.

Model-agnostic and black-box counterfactual generation. A large body of work studies counterfactual generation for black-box predictors through model-agnostic objectives and derivative-free search. Representative examples include MACE Yang et al. (2022), reinforcement-learning-based approaches for scalable black-box recourse Samoilescu et al. (2021), and causally constrained generation methods such as MC3G Dasgupta et al. (2025). Model-agnostic frameworks have also been developed to improve plausibility under complex tabular distributions, such as CountARFactuals Dandl et al. (2024). Genetic and sampling-based optimizers have also been used in other domains, such as molecule counterfactual generation Wellawatte et al. (2022). These methods focus on instance-level recourse, and they do not optimize transport-based distances between empirical input and output distributions.

Distributional counterfactual explanations. Distributional Counterfactual Explanations

(DCE) You et al. (2025) adopt a distribution-level formulation. DCE seeks a counterfactual input distribution that steers the model output distribution toward a target while remaining close to the original population under optimal transport constraints Peyré et al. (2019). It provides a certification mechanism for finite-sample feasibility. The original DCE solver relies on gradient-based optimization and assumes differentiable predictors and pipelines, which restricts direct applicability to pipelines where the predictor and preprocessing are non-differentiable Breiman (2001); Friedman (2001); Shwartz-Ziv and Armon (2022); Erickson et al. (2025).

Distribution-aware counterfactual attribution. Related work has also leveraged distributional information to guide counterfactual explanations at the feature attribution level. For example, You et al. (2026) incorporate joint distribution-informed Shapley values to identify sparse and interpretable counterfactual attributions. While sharing a distribution-aware perspective, these approaches focus on explaining and ranking feature-level interventions, rather than generating counterfactual input distributions or addressing solver design.

Positioning of DISCOVER. DISCOVER builds on the certified OT formulation of DCE while introducing a sparse, propose-and-select distributional search paradigm that does not query model gradients. It makes the sample-level structure induced by transport objectives explicit through per-sample impact scoring, and supports black-box predictors through modular candidate proposals guided by input-side OT geometry. This design extends certified distributional counterfactual explanations to realistic tabular pipelines while keeping the same OT objective and applying the same UCL-based feasibility check as in DCE.

B Theoretical Foundations from Distributional Counterfactual Explanations

This section summarizes the key theoretical foundations of DCE that are inherited by DISCOVER.

B.1 Optimal Transport and Sliced Wasserstein

DCE formulates distributional counterfactual explanations by measuring input proximity and output alignment via optimal transport (OT). For one-dimensional distributions γ_1, γ_2 , the squared 2-Wasserstein distance is defined as

$$\mathcal{W}^2(\gamma_1, \gamma_2) \triangleq \inf_{\pi \in \Pi(\gamma_1, \gamma_2)} \int_{\mathbb{R} \times \mathbb{R}} \|a_1 - a_2\|^2 d\pi(a_1, a_2), \quad (9)$$

where $\Pi(\gamma_1, \gamma_2)$ is the set of transport plans with marginals γ_1 and γ_2 [You et al. (2025), Eq. (1)].

For high-dimensional inputs, DCE uses the sliced Wasserstein distance, which averages 1D Wasserstein distances over random projections:

$$\mathcal{SW}^2(\gamma_1, \gamma_2) \triangleq \int_{\mathbb{S}^{d-1}} \mathcal{W}^2(\theta_{\#}\gamma_1, \theta_{\#}\gamma_2) d\sigma(\theta), \quad (10)$$

where σ is the uniform measure on the unit sphere and $\theta_{\#}$ denotes the push-forward under projection [You et al. (2025), Eq. (2)]. This choice preserves a quantile-based interpretation while enabling scalable computation.

DCE casts distributional counterfactual generation as a chance-constrained problem. Given a factual input distribution x' and a model $b: \mathbb{R}^d \rightarrow \mathbb{R}$, let $y' = b(x')$ be the factual output distribution and let y^* be a target output distribution. DCE seeks a counterfactual input distribution x that is close to x' while producing outputs close to y^* :

$$\max_{x, P} P \quad (11)$$

$$\text{s.t. } P \leq \mathbb{P}[\mathcal{SW}^2(x, x') < U_x], \quad (12)$$

$$P \leq \mathbb{P}[\mathcal{W}^2(b(x), y^*) < U_y], \quad (13)$$

$$P \geq 1 - \frac{\alpha}{2}, \quad (14)$$

[You et al. (2025), Eq. (3)]. The output-side Wasserstein distance admits an explicit quantile form. With $y = b(x)$,

$$\mathcal{W}^2(y, y^*) = \int_0^1 (F_y^{-1}(q) - F_{y^*}^{-1}(q))^2 dq, \quad (15)$$

which directly compares matched quantiles of the two output distributions [You et al. (2025), Eq. (4)].

DCE also shows that the empirical estimation error rate for \mathcal{SW}^2 matches that of the 1D \mathcal{W}^2 estimator under its assumptions. Formally, if \mathcal{W}^2 admits sample complexity $\xi(n)$ for 1D empirical estimation, then \mathcal{SW}^2 admits the same $\xi(n)$ in \mathbb{R}^d [You et al. (2025), Proposition 3.1]. DISCOVER inherits these OT quantities, since its solver still evaluates candidate distributions using the same $\mathcal{SW}^2(x, x')$ and $\mathcal{W}^2(b(x), y^*)$.

B.2 Upper Confidence Limits for Certification

To certify feasibility under finite samples, DCE derives upper confidence limits (UCLs) for both the output-side $\mathcal{W}^2(b(x), y^*)$ and the input-side $\mathcal{SW}^2(x, x')$. Let $\delta \in (0, \frac{1}{2})$ be a trimming constant. DCE provides a uniform confidence statement (with level $1 - \alpha/2$) for the following UCL forms [You et al. (2025), Theorem 3.2].

For the output-side Wasserstein term, define

$$D(u) \triangleq \max \left\{ F_{y,n}^{-1}(\bar{q}_{\alpha,n}(u)) - F_{y^*,n}^{-1}(\underline{q}_{\alpha,n}(u)), \right. \\ \left. F_{y^*,n}^{-1}(\bar{q}_{\alpha,n}(u)) - F_{y,n}^{-1}(\underline{q}_{\alpha,n}(u)) \right\}. \quad (16)$$

[You et al. (2025), Eq. (7)]. Then, with probability at least $1 - \alpha/2$,

$$\mathcal{W}^2(b(x), y^*) \leq \frac{1}{1 - 2\delta} \int_{\delta}^{1-\delta} D(u) du, \quad (17)$$

[You et al. (2025), Eq. (6)]. DCE denotes the right-hand side as an output-side UCL and checks feasibility by requiring

$$\bar{\mathcal{W}}^2 \triangleq \frac{1}{1 - 2\delta} \int_{\delta}^{1-\delta} D(u) du \leq U_y, \quad (18)$$

[You et al. (2025), Eq. (10)].

For the input-side sliced Wasserstein term, let $\theta_1, \dots, \theta_N$ be i.i.d. projection vectors and let σ_N be the corresponding empirical measure. Define

$$D_{\theta,n}(u) \triangleq \max \left\{ F_{\theta^\top x,n}^{-1}(\bar{q}_{\alpha,n}(u)) - F_{\theta^\top x',n}^{-1}(\underline{q}_{\alpha,n}(u)), \right. \\ \left. F_{\theta^\top x',n}^{-1}(\bar{q}_{\alpha,n}(u)) - F_{\theta^\top x,n}^{-1}(\underline{q}_{\alpha,n}(u)) \right\}. \quad (19)$$

[You et al. (2025), Eq. (9)]. Then, with probability at least $1 - \alpha/2$,

$$\mathcal{SW}^2(x, x') \leq \frac{1}{1 - 2\delta} \int_{\mathbb{S}^{d-1}} \int_{\delta}^{1-\delta} D_{\theta,N}(u) du d\sigma_N(\theta), \quad (20)$$

[You et al. (2025), Eq. (8)]. DCE denotes the right-hand side as an input-side UCL and checks feasibility by requiring

$$\bar{\mathcal{SW}}^2 \triangleq \frac{1}{1 - 2\delta} \int_{\mathbb{S}^{d-1}} \int_{\delta}^{1-\delta} D_{\theta,N}(u) du d\sigma_N(\theta) \leq U_x, \quad (21)$$

[You et al. (2025), Eq. (11)].

These UCLs operationalize the chance constraints in the DCE formulation while remaining independent of the particular solver. DISCOVER inherits the same certification step by applying the same UCL computations to candidate counterfactual distributions.

B.3 Riemannian BCD Objective and Interval Narrowing

DCE solves the chance-constrained formulation by optimizing a weighted objective that balances input proximity and output alignment. Let $x = \{x_i\}_{i=1}^n$ be an empirical counterfactual input distribution and let

$y^* = \{y_j^*\}_{j=1}^n$ be an empirical target output distribution. With projection set $\Theta = \{\theta_k\}_{k=1}^N$, DCE defines the empirical OT objectives (we use the standard $1/N$ normalization for the Monte Carlo approximation of \overline{SW}^2)

$$Q_x(x, \mu) \triangleq \frac{1}{N} \sum_{k=1}^N \sum_{i=1}^n \sum_{j=1}^n \|\theta_k^\top x_i - \theta_k^\top x'_j\|^2 \mu_{ij}^{(k)}, \quad (22)$$

$$Q_y(x, \nu) \triangleq \sum_{i=1}^n \sum_{j=1}^n \|b(x_i) - y_j^*\|^2 \nu_{ij}, \quad (23)$$

[You et al. (2025), Eq. (12)–(13)]. For a fixed balance parameter $\eta \in [0, 1]$, DCE combines them as

$$Q(x, \mu, \nu, \eta) \triangleq (1 - \eta) \cdot Q_x(x, \mu) + \eta \cdot Q_y(x, \nu), \quad (24)$$

[You et al. (2025), Eq. (15)].

A key theoretical point in DCE is that, under feasibility, there exists an $\eta^* \in [0, 1]$ such that minimizing $Q(\cdot, \eta^*)$ yields an optimal solution of the original constrained problem [You et al. (2025), Theorem 4.1]. This motivates dynamically adapting η rather than fixing it.

DCE computes η from the UCL gaps and then refines a feasible interval $[l, r]$ across iterations. Let

$$a = U_x - \overline{SW}^2, \quad b = U_y - \overline{W}^2,$$

where \overline{SW}^2 and \overline{W}^2 are the UCLs defined above [You et al. (2025), Eq. (10)–(11)]. DCE specifies the balancing rule

$$\eta = \begin{cases} \frac{b}{a+b}, & \text{if } a \text{ and } b \text{ are both negative,} \\ \frac{a}{a+b}, & \text{if } a \text{ and } b \text{ are both non-negative,} \\ 0.5, & \text{if } a = b = 0, \end{cases} \quad (25)$$

[You et al. (2025), Eq. (25)]. This rule assigns more weight to the side that is either more violated (both negative case) or closer to violation (both non-negative case) [You et al. (2025), Appendix D].

After computing η , DCE applies Interval Narrowing (Algorithm 2) to update the interval $[l, r]$. We restate the interval narrowing procedure from DCE for completeness [You et al. (2025), Algorithm 2].

In DCE, the interval $[l, r]$ and κ are carried across runs so that η is refined progressively rather than changing abruptly [You et al. (2025), Algorithm 2 and the discussion around it]. DISCOVER inherits this balancing principle. Even though DISCOVER replaces gradient-based updates with solver-driven

Algorithm 4 Interval Narrowing

Require: \overline{SW}^2 , \overline{W}^2 , U_x, U_y , $[l, r]$, and κ ($0 < \kappa < 1$)

Ensure: η

- 1: $\eta \leftarrow$ Balance the gaps \overline{SW}^2 and \overline{W}^2
 - 2: **if** $\eta > (l + r)/2$ **then**
 - 3: $l \leftarrow l + \kappa(r - l)$
 - 4: **else**
 - 5: $r \leftarrow r - \kappa(r - l)$
 - 6: **end if**
 - 7: Save $[l, r]$ and κ as the input for the next run
 - 8: **return** η
-

candidate search, it still uses the same two UCL gaps, the same η balancing rule, and the same interval narrowing mechanism to maintain the intended trade-off between input proximity and output alignment.

C Key Properties of DISCOVER

This section provides short proofs for the two key properties stated in the main text.

C.1 Proof of Proposition 3.1

By definition,

$$q_i^{(x)} = \frac{1}{N} \sum_{k=1}^N \sum_{j=1}^n |\theta_k^\top x_i - \theta_k^\top x'_j|^2 \mu_{ij}^{(k)}.$$

Summing over i and reordering the summations gives

$$\sum_{i=1}^n q_i^{(x)} = \frac{1}{N} \sum_{k=1}^N \sum_{i=1}^n \sum_{j=1}^n |\theta_k^\top x_i - \theta_k^\top x'_j|^2 \mu_{ij}^{(k)} = Q_x(x, \mu).$$

Similarly, using the definition

$$q_i^{(y)} = \sum_{j=1}^n |b(x_i) - y_j^*|^2 \nu_{ij},$$

we obtain $\sum_{i=1}^n q_i^{(y)} = Q_y(x, \nu)$. Finally,

$$\begin{aligned} \sum_{i=1}^n q_i &= (1 - \eta) \sum_{i=1}^n q_i^{(x)} + \eta \sum_{i=1}^n q_i^{(y)} \\ &= (1 - \eta) Q_x(x, \mu) + \eta Q_y(x, \nu) = Q(x, \mu, \nu, \eta). \end{aligned}$$

C.2 Proof of Proposition 3.2

Let $X^{(0)} = X$ be the no-op proposal included in the candidate set. By construction,

$$\begin{aligned} Q(\widehat{X}; \eta) &= \min_{m \in \{0, 1, \dots, M\}} Q(X^{(m)}; \eta) \\ &\leq Q(X^{(0)}; \eta) \\ &= Q(X; \eta). \end{aligned}$$

Therefore the propose-and-select step is monotone (non-increasing) in the certified objective for the fixed η used during candidate evaluation.

D Additional Ablation Results

Table 4 reports additional ablations for two solver hyperparameters. We vary the within-row update size h under the Monte Carlo strategy and the intervention budget k under the Genetic strategy, while keeping the remaining components fixed.

Effect of h . Increasing h expands the local proposal scope within each selected sample. Across datasets, larger h tends to reduce $OT(y)$ more quickly, but it can increase $OT(x)$ and MMD when proposals become less local. This behavior directly reflects the role of the OT-guided cone sampler: DISCOVER is most effective when proposals remain transport-consistent rather than performing large unconstrained jumps. The best trade-off often occurs at intermediate values, suggesting that h primarily controls exploration scale within the propose-and-select framework.

Effect of k . The budget k controls how many samples can be edited per iteration. On heterogeneous datasets, larger k can reduce $OT(y)$ in some settings, but it also increases variance and can worsen $OT(x)$. This supports the core sparsity mechanism of DISCOVER: distributional alignment is achieved through targeted top- k interventions, rather than uniformly shifting the full population. Overall, these results justify using a small intervention budget to stabilize certified distribution-level search under black-box predictors.

E Qualitative Analysis of Distributional Counterfactuals

This section provides qualitative visualizations to complement the quantitative evaluation in the main paper.

E.1 Distributional Shifts across Datasets

Figure 6 visualizes how DISCOVER reshapes empirical input and output distributions across datasets with mixed feature types. For numerical features and prediction scores, DISCOVER shifts the empirical CDFs toward the target while largely preserving the overall shape of the factual distributions, which is consistent with low input-side transport distortion. For categorical features, frequency changes are concentrated on a small number of categories, rather than spreading mass broadly across many levels.

Across datasets, the counterfactual outputs move toward the target distribution while the input distributions remain close to the factual reference. These

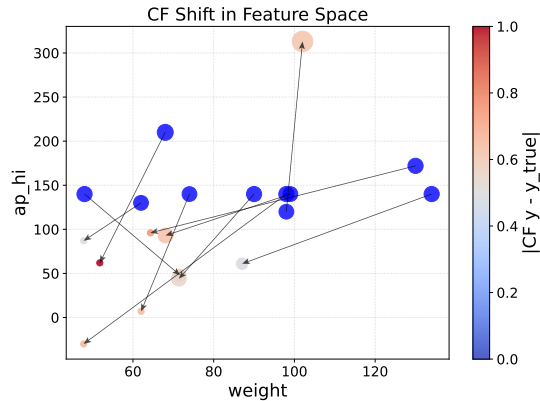


Figure 5: Sample-level counterfactual shifts produced by DISCOVER on the Cardio dataset. Points denote factual (blue) and counterfactual (red) samples in the weight–systolic blood pressure plane, with arrows indicating the update direction and magnitude. Point size encodes diastolic blood pressure (ap_{lo}), and color reflects the corresponding reduction in predicted risk.

visual patterns align with the OT-based metrics reported in the main results and provide an interpretable view of distribution-level recourse.

E.2 Sample-Level Counterfactual Shifts in Feature Space

Figure 5 illustrates sample-level movements induced by DISCOVER in the input space. Arrows visualize the change from each factual instance to its counterfactual counterpart, while color encodes the absolute change in model output, $|b(x) - b(x')|$.

Two patterns are consistent with the solver design. First, most updates remain local, and larger movements are concentrated on a subset of samples, which matches the top- k intervention mechanism. Second, samples with larger output changes typically exhibit larger input displacements, indicating that distribution-level alignment is achieved through targeted edits rather than uniform shifts of the entire population.

E.3 Dynamic Reweighting of Sample Contributions

Figure 7 shows $q_i(t)$ when samples are ordered by long-run top- k selection frequency. Because the colormap is normalized per iteration, the figure highlights how the solver concentrates attention within each iteration. A small set of samples is repeatedly selected, which indicates persistent influential contributors under the current transport coupling. At the same time, non-selected samples still exhibit non-

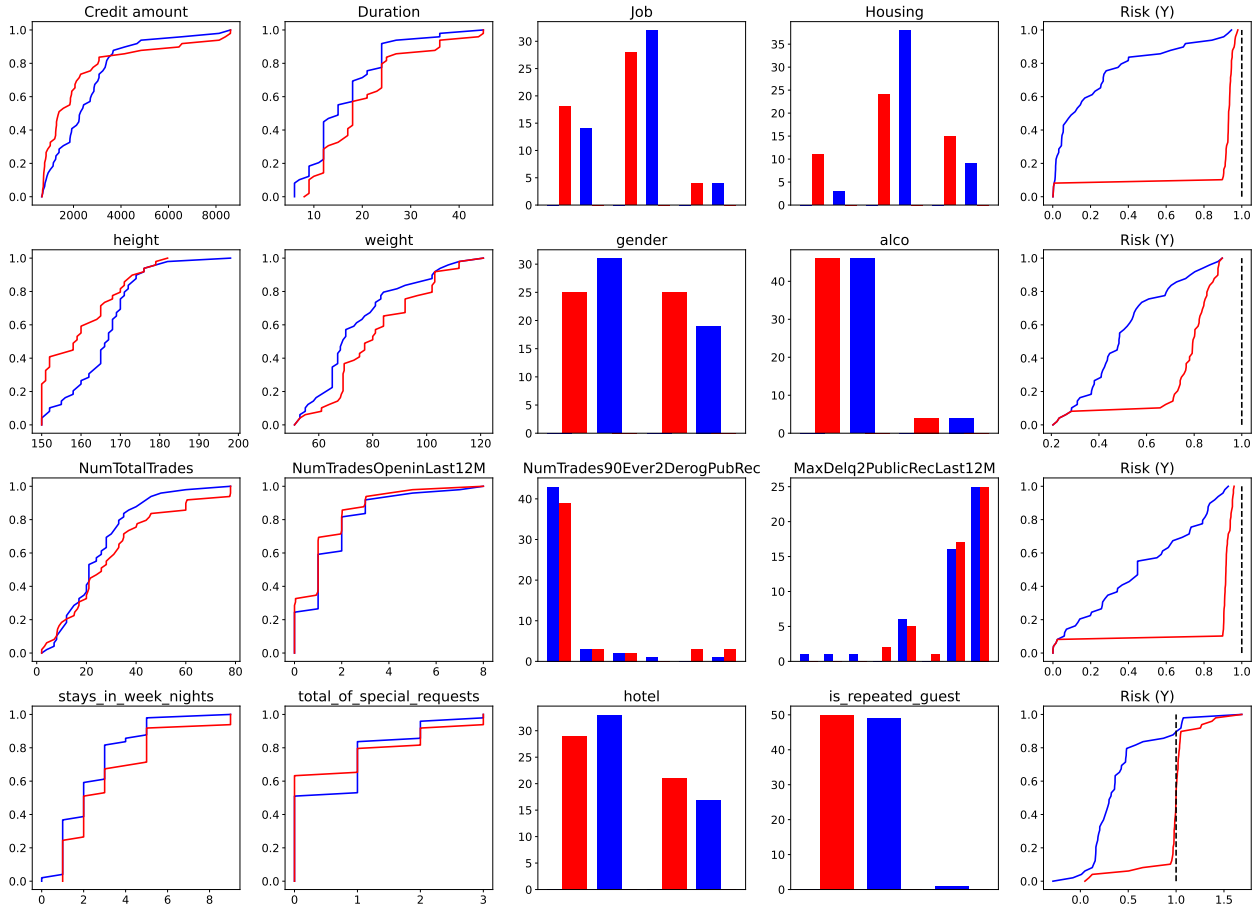


Figure 6: Empirical distribution visualizations of factual and counterfactual samples generated by DISCOVER on German Credit, Cardio, HELOC, and Hotel Booking. For numerical features and model outputs Y , curves show empirical CDFs with the horizontal axis representing feature values or risk scores. For categorical features, bar plots indicate empirical frequencies. Gray curves correspond to factual distributions, dashed black curves denote target output distributions when applicable, and colored curves represent DISCOVER counterfactuals.

zero scores, since $q_i(t)$ is evaluated for all samples before top- k gating.

Figure 8 shows the same trajectories under an initialization-based ordering and a global color scale. Early iterations concentrate mass on initially influential samples, but top- k membership changes over time, which indicates that influence is not fixed by initialization. The global scale also reveals a decrease in the overall magnitude of $q_i(t)$, which is consistent with a reduction in transport discrepancy as optimization progresses.

Overall, these visualizations show that DISCOVER combines global reweighting of sample influence with sparse top- k interventions. This mechanism concentrates edits on samples that contribute most to the current transport discrepancy while maintaining a stable distribution-level optimization process.

E.4 Computational Complexity of DISCOVER

Notation. Let n be the number of samples in the empirical distribution, d the number of input features, N the number of random projection directions used to approximate the sliced Wasserstein distance, T the number of outer iterations, M the number of candidate proposals per iteration, k the top- k intervention budget (number of editable rows per iteration), and h the number of edited features per selected row (a within-row update budget). For categorical feature p , let $|V_p|$ be its number of discrete values and let r be the embedding dimension used in the categorical proposal step. Let C_b denote the cost of one forward call to the predictor $b(\cdot)$ on a single sample (model-query cost; for vectorized inference C_b can be interpreted as amortized per-sample cost).

Table 4: Ablation results under Monte Carlo (MC) and Genetic strategies on four datasets. Panel A varies the step-size parameter h under MC and reports mean \pm 95% CI over five seeds. Panel B varies the top- k parameter under the Genetic strategy and reports mean \pm 95% CI over the three random seeds shared across $k \in \{3, 10, 20\}$ (to ensure consistent comparison across k settings). For each dataset and model, the best value (lowest mean) for each metric within a panel is highlighted in bold.

Dataset	h	MLP				Random Forest			
		OT(x)	OT(y)	MMD	AReS Cost	OT(x)	OT(y)	MMD	AReS Cost
German Credit	$h = 1$	0.0837 \pm 0.0176	0.0196 \pm 0.0307	0.0310\pm0.0049	6.59\pm0.78	0.1102\pm0.0281	0.1014 \pm 0.0454	0.0353\pm0.0038	7.81\pm1.31
	$h = 2$	0.0845 \pm 0.0265	0.0058 \pm 0.0072	0.0343 \pm 0.0041	7.20 \pm 1.13	0.1258 \pm 0.0234	0.0680 \pm 0.0207	0.0400 \pm 0.0035	8.30 \pm 0.58
	$h = 4$	0.0799 \pm 0.0117	0.0019 \pm 0.0011	0.0373 \pm 0.0039	8.94 \pm 0.61	0.1216 \pm 0.0229	0.0571 \pm 0.0217	0.0425 \pm 0.0050	10.05 \pm 0.81
	$h = 8$	0.0778\pm0.0183	0.0011\pm0.0007	0.0458 \pm 0.0088	10.54 \pm 1.58	0.1124 \pm 0.0239	0.0372\pm0.0109	0.0512 \pm 0.0123	12.28 \pm 2.51
COMPAS	$h = 1$	0.1128\pm0.0296	0.0313 \pm 0.0083	0.0541\pm0.0099	9.95\pm2.30	0.0559\pm0.0176	0.0210 \pm 0.0065	0.0247\pm0.0078	8.42 \pm 3.29
	$h = 2$	0.1149 \pm 0.0245	0.0282 \pm 0.0126	0.0564 \pm 0.0053	10.24 \pm 2.37	0.0615 \pm 0.0131	0.0174 \pm 0.0049	0.0284 \pm 0.0063	7.75 \pm 1.00
	$h = 4$	0.1385 \pm 0.0813	0.0255 \pm 0.0099	0.0553 \pm 0.0122	10.63 \pm 2.31	0.0720 \pm 0.0144	0.0148 \pm 0.0054	0.0318 \pm 0.0085	7.17 \pm 0.98
	$h = 8$	0.1609 \pm 0.0435	0.0169\pm0.0083	0.0620 \pm 0.0069	10.15 \pm 2.56	0.0739 \pm 0.0180	0.0113\pm0.0039	0.0339 \pm 0.0078	6.96\pm1.08
HELOC	$h = 1$	0.1108\pm0.0220	0.0071 \pm 0.0017	0.0340\pm0.0053	7.25 \pm 0.79	0.0875\pm0.0210	0.0291 \pm 0.0171	0.0266\pm0.0048	4.48\pm0.89
	$h = 2$	0.1335 \pm 0.0453	0.0055 \pm 0.0014	0.0393 \pm 0.0038	7.37 \pm 0.98	0.0983 \pm 0.0201	0.0228 \pm 0.0094	0.0321 \pm 0.0058	4.96 \pm 1.20
	$h = 4$	0.1751 \pm 0.0663	0.0047 \pm 0.0010	0.0405 \pm 0.0041	7.55 \pm 1.02	0.1387 \pm 0.0435	0.0145 \pm 0.0086	0.0337 \pm 0.0065	5.36 \pm 0.93
	$h = 8$	0.1691 \pm 0.0779	0.0035\pm0.0013	0.0445 \pm 0.0056	7.08\pm0.82	0.1220 \pm 0.0406	0.0129\pm0.0093	0.0368 \pm 0.0078	5.09 \pm 1.06
Cardio	$h = 1$	0.0643 \pm 0.0425	0.0134 \pm 0.0080	0.0232 \pm 0.0073	7.21 \pm 2.82	0.0369 \pm 0.0140	0.0107 \pm 0.0035	0.0192\pm0.0039	6.49\pm1.00
	$h = 2$	0.0566 \pm 0.0361	0.0109 \pm 0.0089	0.0234 \pm 0.0051	7.34 \pm 1.55	0.0417 \pm 0.0289	0.0075 \pm 0.0027	0.0212 \pm 0.0036	7.09 \pm 1.57
	$h = 4$	0.0534\pm0.0285	0.0066\pm0.0042	0.0265 \pm 0.0069	8.48 \pm 1.14	0.0347\pm0.0001	0.0071 \pm 0.0039	0.0227 \pm 0.0056	7.80 \pm 1.67
	$h = 8$	0.0544 \pm 0.0241	0.0067 \pm 0.0023	0.0192\pm0.0021	7.13\pm1.28	0.0394 \pm 0.0166	0.0071\pm0.0026	0.0265 \pm 0.0058	8.31 \pm 1.21

Dataset	k	SVM				XGBoost			
		OT(x)	OT(y)	MMD	AReS Cost	OT(x)	OT(y)	MMD	AReS Cost
German Credit	$k = 3$	0.8351\pm0.3131	0.2144\pm0.0387	0.0602 \pm 0.0201	13.96 \pm 1.82	0.0864\pm0.0482	0.0033\pm0.0031	0.0457\pm0.0064	11.35\pm0.75
	$k = 10$	0.8876 \pm 0.5071	0.2192 \pm 0.0295	0.0237 \pm 0.1022	4.43\pm19.08	0.1545 \pm 0.0608	0.0120 \pm 0.0185	0.0467 \pm 0.0015	12.81 \pm 3.36
	$k = 20$	0.8472 \pm 0.4786	0.2387 \pm 0.0822	0.0219\pm0.0942	5.26 \pm 22.63	0.2534 \pm 0.3980	0.0807 \pm 0.0767	0.0537 \pm 0.0128	12.59 \pm 1.71
COMPAS	$k = 3$	0.2660\pm0.1678	0.0100\pm0.0095	0.0866 \pm 0.0021	16.56\pm2.81	0.3091\pm0.5377	0.0177\pm0.0206	0.0636 \pm 0.0241	17.37\pm9.39
	$k = 10$	0.4979 \pm 0.1041	0.0288 \pm 0.0162	0.0705\pm0.0090	18.53 \pm 4.48	0.3422 \pm 0.4806	0.0326 \pm 0.0254	0.0795 \pm 0.0318	20.35 \pm 6.61
	$k = 20$	0.4302 \pm 0.3002	0.0590 \pm 0.0597	0.0899 \pm 0.0084	19.03 \pm 7.88	0.4080 \pm 0.3655	0.0628 \pm 0.0785	0.0592\pm0.0284	19.67 \pm 3.63
HELOC	$k = 3$	0.1888 \pm 0.1623	0.0574 \pm 0.0195	0.0620 \pm 0.0051	11.15\pm0.88	0.0869\pm0.0164	0.0051\pm0.0028	0.0450 \pm 0.0042	5.72\pm0.25
	$k = 10$	0.1857\pm0.1464	0.0390\pm0.0104	0.0554\pm0.0065	11.77 \pm 1.13	0.1185 \pm 0.0284	0.0083 \pm 0.0051	0.0395\pm0.0030	6.12 \pm 0.47
	$k = 20$	0.3701 \pm 0.3532	0.0501 \pm 0.0332	0.0700 \pm 0.0067	13.46 \pm 3.09	0.1003 \pm 0.0331	0.0149 \pm 0.0079	0.0412 \pm 0.0058	6.37 \pm 0.67
Cardio	$k = 3$	0.0435\pm0.0260	0.0040 \pm 0.0022	0.0180\pm0.0033	10.57\pm1.12	0.0553 \pm 0.0472	0.0033 \pm 0.0025	0.0256 \pm 0.0057	11.19\pm0.85
	$k = 10$	0.0558 \pm 0.0304	0.0035\pm0.0021	0.0209 \pm 0.0062	11.23 \pm 1.29	0.0431\pm0.0329	0.0027\pm0.0015	0.0219\pm0.0044	12.47 \pm 1.55
	$k = 20$	0.0619 \pm 0.0480	0.0046 \pm 0.0031	0.0268 \pm 0.0072	13.20 \pm 1.48	0.0502 \pm 0.0388	0.0043 \pm 0.0038	0.0253 \pm 0.0058	13.29 \pm 1.82

One-time precomputation. Because the factual distribution X' and target outputs Y^* are fixed, we can precompute: (i) for each projection θ_k ($k = 1, \dots, N$), the projected factual scalars $\{\theta_k^\top x'_j\}_{j=1}^n$ and their sorted order; and (ii) the sorted target outputs $\{y_j^*\}_{j=1}^n$. This costs

$$\mathcal{O}(N(nd + n \log n) + n \log n)$$

time and stores $\mathcal{O}(Nn)$ projected scalars (plus indices).

Cost of evaluating the certified objective on one distribution. Evaluating the certified objective $Q(X; \eta) = (1-\eta)Q_x(X) + \eta Q_y(X)$ on a candidate empirical distribution X requires:

- **Input-side SW_2 :** for each projection θ_k , compute $\{\theta_k^\top x_i\}_{i=1}^n$ ($\mathcal{O}(nd)$), sort the projected values ($\mathcal{O}(n \log n)$), and compute the 1D OT cost and UCL terms via rank-matching ($\mathcal{O}(n)$). Thus, for N projections,

$$\mathcal{O}(N(nd + n \log n)).$$

- **Output-side W_2 :** evaluate the predictor on all samples $y_i = b(x_i)$ ($\mathcal{O}(nC_b)$), sort $\{y_i\}_{i=1}^n$ ($\mathcal{O}(n \log n)$), and compute the 1D

OT cost and UCL terms ($\mathcal{O}(n)$). Overall,

$$\mathcal{O}(nC_b + n \log n).$$

Therefore, a full evaluation of $Q(X; \eta)$ (including the UCL-based feasibility checks used to update η) costs

$$\mathcal{O}(N(nd + n \log n) + nC_b + n \log n). \quad (26)$$

Per-iteration cost of DISCOVER (worst-case, recomputing from scratch). At outer iteration t , DISCOVER performs:

1. **Evaluate $Q(X_t; \eta_t)$ and update η_t :** one call to equation 26.
2. **Compute per-row impact scores and select top- k :** given the rank-matching structure produced while computing SW_2 and W_2 , the per-row contributions can be accumulated in $\mathcal{O}(Nn + n)$ time (plus a top- k selection that is $\mathcal{O}(n)$ expected via selection, or $\mathcal{O}(n \log n)$ if fully sorting). This does not change the leading-order term of equation 26.
3. **Compute the input-side guidance field g :** if we materialize a full gradient-like field $g \in \mathbb{R}^{n \times d}$ from the sliced OT matches,

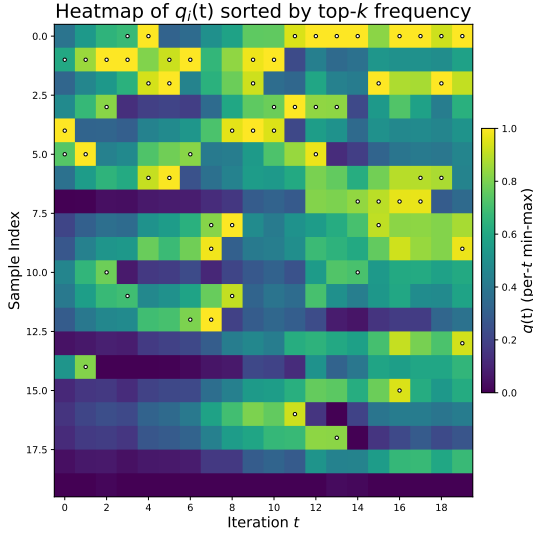


Figure 7: Heatmap of $q_i(t)$ with samples sorted by their top- k selection frequency across iterations ($k=3$, 20 samples shown). The horizontal axis denotes the iteration index t . The vertical axis corresponds to sample indices after sorting by how frequently each sample appears in the top- k set over all iterations. Color encodes $q_i(t)$ using per-iteration min-max normalization, so the colormap emphasizes relative importance within each iteration. White circular markers indicate samples selected into the top- k set at iteration t .

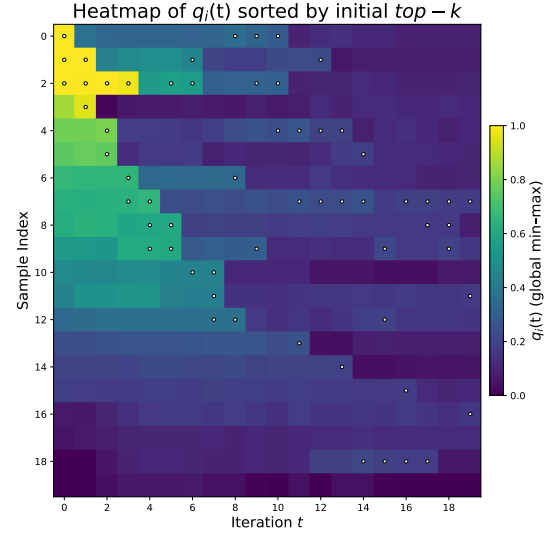


Figure 8: Heatmap of $q_i(t)$ with samples sorted by their initial ranking induced by $q_i(0)$ ($k=3$, 20 samples shown). The horizontal axis denotes the iteration index t . The vertical axis corresponds to sample indices ordered by the initial ranking, with initial top- k samples appearing at the top. Color encodes $q_i(t)$ using a global min-max scale shared across iterations, which highlights changes in absolute magnitude over time. White circular markers indicate samples selected into the top- k set at iteration t .

the accumulation across N projections costs $\mathcal{O}(Nnd)$. (If guidance is only needed on the editable set I of size k , this reduces to $\mathcal{O}(Nkd)$; see below.)

4. **Generate M candidates (proposal step):** each proposal edits only k rows and h features per row. For numerical edits, this costs $\mathcal{O}(Mkh)$. For categorical edits, decoding may require scanning all categories in edited features, yielding $\mathcal{O}\left(Mk \sum_{p \in \mathcal{C}_{\text{edit}}} |V_p| r\right)$ in the worst case, where $\mathcal{C}_{\text{edit}}$ denotes the set of edited categorical features.
5. **Select the best candidate via certified objective:** naively, DISCOVER evaluates $Q(\cdot; \eta_t)$ for each candidate $X_t^{(m)}$ ($m = 1, \dots, M$), which costs M additional calls to equation 26.

Putting the dominant terms together, the worst-case per-iteration time complexity is

$$\mathcal{O}\left((M+1)\left(N(nd+n \log n) + nC_b + n \log n\right) + Nnd + Mkh\right) \quad (27)$$

where the Nnd term corresponds to computing a dense guidance field g . In practice, the proposal-generation cost Mkh is typically dominated by candidate scoring unless M is extremely small.

Hence the total worst-case runtime over T iterations is

$$\mathcal{O}\left(T(M+1)\left(N(nd+n \log n) + nC_b + n \log n\right)\right) \quad (\text{dominant term}).$$

Sparsity-aware amortized cost (recommended implementation). The top- k intervention budget implies that each candidate differs from X_t in only k rows. This permits two practical optimizations that reduce constant factors and, with additional data structures, can also reduce asymptotic costs:

- **Sparse guidance:** compute guidance only on the editable set I , reducing the guidance construction from $\mathcal{O}(Nnd)$ to $\mathcal{O}(Nkd)$.
- **Incremental model queries:** because only k rows change, one can cache $y_i = b(x_i)$ for the current iterate and re-evaluate $b(\cdot)$ only on edited rows for each candidate, reducing

model calls from $\mathcal{O}(nC_b)$ to $\mathcal{O}(kC_b)$ per candidate. The output-side sorting step remains $\mathcal{O}(n \log n)$ if recomputed from scratch, but can be updated in $\mathcal{O}(k \log n)$ if maintaining an order-statistics structure.

- **Incremental projections:** similarly, projected values $\theta_k^\top x_i$ can be cached and updated only for edited rows, reducing projection computation from $\mathcal{O}(Nnd)$ to $\mathcal{O}(Nkd)$ per candidate. As above, sorting can be recomputed from scratch ($\mathcal{O}(Nn \log n)$) or incrementally updated ($\mathcal{O}(Nk \log n)$) with balanced-tree / order-statistics maintenance per projection.

Under caching and incremental updates with recomputed sorting (a conservative middle ground), the per-candidate evaluation cost becomes

$$\mathcal{O}(N(kd + n \log n) + kC_b + n \log n),$$

while the dense-from-scratch baseline remains equation 26. If incremental sorting is used, the $n \log n$ terms can be replaced by $k \log n$ in both the input and output sides.

Space complexity. Storing the current distribution $X \in \mathbb{R}^{n \times d}$ requires $\mathcal{O}(nd)$ memory. Caching projected scalars for N projections requires $\mathcal{O}(Nn)$ memory, and storing the predictor outputs requires $\mathcal{O}(n)$. Per-row scores require $\mathcal{O}(n)$. A dense guidance field $g \in \mathbb{R}^{n \times d}$ costs $\mathcal{O}(nd)$ memory, but can be avoided by computing guidance only for the editable set, reducing storage to $\mathcal{O}(kd)$.

Algorithm 1 is written as if all M candidates are materialized; that would require $\mathcal{O}(Mnd)$ memory. However, a streaming implementation that generates and scores candidates one-by-one only needs to keep the best-so-far candidate, reducing memory to $\mathcal{O}(nd + Nn)$ (plus caches and small proposal buffers).

F Reproducibility and Configuration Details

To support reproducibility, experiments in this work are driven by explicit configuration files and executable scripts. All experiments can be reproduced. In particular, baseline comparison experiments are executed through provided notebooks, while ablation studies are conducted using Python scripts with structured JSON-based configuration files. Baseline methods are evaluated using their original implementations, following the default or recommended parameter settings provided by the respective authors. Consequently, baseline hyper-parameters are not globally fixed across datasets, which is consistent

with common practice in counterfactual explanation benchmarks.

For DISCOVER, parameter choices are structured to isolate the effect of individual components. In ablations of the OT-guided cone sampling mechanism, both the intervention budget and the within-sample update budget are fixed to $k = 1$ and $h = 3$, respectively. This ensures that observed differences are attributable solely to the presence or absence of cone guidance. Cone sampling is evaluated under four variants: full guidance, continuous-only, categorical-only, and no guidance, using a shared candidate generation budget and the Monte Carlo proposal strategy on all five datasets.

In experiments analyzing sparse intervention budgets, the cone sampling configuration is held fixed and applied uniformly to both continuous and categorical features. We then study the effects of top- k and h through separate controlled sweeps. Specifically, in the h -ablation, the top- k intervention budget is kept fixed while varying the number of features updated within each selected sample over $h \in \{1, 4, 8\}$. Conversely, in the top- k ablation, the within-sample update budget h is fixed while varying the number of edited samples per iteration over top- $k \in \{3, 10, 20\}$. These ranges are chosen to cover both conservative and more aggressive intervention regimes while maintaining sparse but non-trivial distributional updates. Both Monte Carlo and Genetic optimizers are evaluated under these budgeted configurations on four datasets.

All quantitative results are averaged over multiple random seeds. Cone-sampling ablations use three independent runs per setting, while experiments involving top- k and h variations use five independent runs per setting to ensure stability of the reported distribution-level OT metrics.